JPE 18-1-10

https://doi.org/10.6113/JPE.2018.18.1.103
ISSN(Print): 1598-2092 / ISSN(Online): 2093-4718

Model-free Deadbeat Predictive Current Control of a Surface-mounted Permanent Magnet Synchronous Motor Drive System

Yanan Zhou*, Hongmei Li†, and Hengguo Zhang*

*,†Department of Electrical Engineering and Automation, Hefei University of Technology, Hefei, China

Abstract

Parametric uncertainties and inverter nonlinearity exist in the permanent magnet synchronous motor (PMSM) drive system of electrical vehicles, which may lead to performance degradation or failure, and eventually threaten reliable operation. Therefore, a model-free deadbeat predictive current controller (MFDPCC) for PMSM drive systems is proposed in this study. The data-driven ultra-local model of a surface-mounted PMSM (SMPMSM) drive system that consists of parametric uncertainties and inverter nonlinearity is first established through the input and output data of a SMPMSM drive system. Subsequently, MFDPCC is designed. The performance comparisons and analyses of the proposed MFDPCC, the conventional proportional–integral controller, and the model-based deadbeat predictive current controller for SMPMSM drive systems are implemented via system simulation and experimental tests. Results show the effectiveness and technical advantages of the proposed MFDPCC.

Key words: Inverter nonlinearity, Parametric uncertainties, PMSM, Predictive current control

I. INTRODUCTION

Permanent magnet synchronous motors (PMSMs) have been widely applied to the traction systems of electric vehicles (EVs). The commonly used control mode is torque control with only a current loop. Notably, PMSM drive systems involve parametric uncertainties and inverter nonlinearity [1], [2].

The proportional–integral (PI) controller remains the most commonly used controller for PMSM drive systems in EVs due to its simple structure and easy implementation. However, the performance of PI-controlled PMSM drive systems can be seriously degraded under parametric uncertainties and inverter nonlinearity because the design of controller parameters heavily depends on an accurate mathematical model of PMSM system.

Predictive control exhibits the advantages of clear concept, high dynamic performance, easy implementation, and zero-offset control in theory. Therefore, predictive control has emerged as a useful algorithm for implementing PMSM control with considerable potential [3]. In addition, the experimental evaluation of finite control set model predictive current control (FCSMPC) and predictive torque control was conducted in [4]. Comparative research among FCSMPC, two-configuration predictive current control, and deadbeat predictive current control was presented in [5]. Deadbeat predictive control leads to fixed switching frequency, low current harmonics, and excellent dynamic and static performance that are suitable for PMSM systems without parametric uncertainties and inverter nonlinearity.

However, predictive control is essentially a model-based approach in which parametric uncertainties and inverter nonlinearity can cause model mismatch and negatively impact the performance of a predictive-controlled PMSM drive system. Then, current distortion, torque pulsation, current control performance degradation, and unstable operation [6], [7] may occur. Accordingly, the torque safety of PMSM drive system will experience challenges. Previous studies [8] used the PI controller and the predictive controller in parallel. However, these studies did not yield good results because both controllers are sensitive to parametric uncertainties. To improve robustness to stator inductance variation, the targeted current error was changed from zero to

Manuscript received Jun. 8, 2017; accepted Sep. 24, 2017
Recommended for publication by Associate Editor Kwang-Woon Lee.
†Corresponding Author: hongmei.li@hfut.edu.cn
Tel: +86-0551-62901618, Hefei University of Technology
*Dept. of Electrical Eng. and Automation, Hefei Univ. of Tech., China

half the difference of the previous two current errors in [9, 10] or the *dq*-axes weighting factors was introduced into the predictive model [11]. However, the variation of the remaining parameters and inverter nonlinearity were not addressed.

Many approaches, such as updating the predictive model continuously based on online multi-parameter estimation [12]-[14] or using a feedforward term to cancel the influence caused by parametric uncertainties based on a disturbance observer, have been proposed to counteract multiple parametric uncertainties [15]-[17]. However, control structures are complex and are all dependent on the accurate measurement of stator voltages. *dq*-Axes stator voltages are difficult to measure, and synchronous sampling with *dq*-axes stator currents are difficult to achieve when *dq*-axes stator voltages are replaced with the reference values of the pulse-width modulation (PWM) inverter. The reasonable compensation of inverter nonlinearity under parametric uncertainties will become a significant challenge.

Other studies have suggested establishing a predictive model based on the current difference detection technology at each sampling period [18]-[20]. The scheme presented in [18] is independent of PMSM parameters but relevant to the measurement precision of stator current. Therefore, high-speed current sampling was executed by a field-programmable gate array. In [19], [20], model-free predictive current control based on FCSMPC was proposed for the first time. The previous current differences under possible voltage vectors were measured and used to predict the future stator current. However, this method requires twice current sampling at each control period. The scheme was improved in [21] with only once current sampling per control period. A similar approach has been adopted for synchronous reluctance motors [22].

Apart from the aforementioned efforts, the mathematical model of PMSM drive system was improved to implement FCSMPC, which allowed for inverter dead time [23]. In [24], dead time and magnetic saturation were considered in the predictive model. However, the reliability of the model is subject to the finite element analysis (FEA) results of PMSM.

From the preceding studies, approaches [19]-[22] for a model-free predictive current controller that focuses only on parametric uncertainties rather than on inverter nonlinearity have been proposed. In [24], the FEA model may not agree with PMSM in practice. Model-free control is robust to uncertainties without requiring a mathematical model of controlled system, such as active disturbance rejection control [25], model-free adaptive control [26], and model-free control (MFC) [27]. MFC has been proposed and applied to several areas based on the data-driven ultra-local model, such as DC-motor servo systems [28], laboratory manipulators [29], magnetic bearings [30], aerodynamic systems [31], greenhouses [32], and electro-hydraulic systems [33]. Moreover, deadbeat predictive current control has many advantages in cases with full knowledge of PMSM drive systems.

Therefore, a data-driven ultra-local model of surface-mounted PMSM (SMPMSM) drive system that allows for parametric uncertainties and inverter nonlinearity is first established based on the input and output data of the SMPMSM drive system, with the reference voltages of the inverter used as the input data. The development of the ultra-local model of SMPMSM drive system not only avoids the measurement of stator voltages and synchronous sampling with stator currents, but also considers the effects of inverter nonlinearity and parametric uncertainties. Then, a model-free deadbeat predictive current controller (MFDPCC) is presented through the innovative integration of the ultra-local model and deadbeat predictive current control, and the guidelines for selecting controller parameters are determined. Finally, system simulation and experimental research are conducted on the proposed SMPMSM drive system. A comparative analysis with the feedforward decoupling PI current-controlled and the model-based deadbeat predictive current-controlled SMPMSM drive systems is performed, and valuable conclusions are drawn.

II. MFDPCC FOR SMPMSM DRIVE SYSTEMS

A. Mathematical Model of SMPMSM with Parametric Uncertainties and Inverter Nonlinearity

The dynamic model of SMPMSM in rotating synchronous reference frame with parametric uncertainties and inverter nonlinearity is given as [34]

$$\begin{cases} \dfrac{di_d}{dt} = \dfrac{1}{L_s}u_d^* - \dfrac{R_s}{L_s}i_d + n_p\Omega_r i_q - \dfrac{1}{L_s}\left(V_{d,par} + V_{d,dead}\right) \\ \dfrac{di_q}{dt} = \dfrac{1}{L_s}u_q^* - \dfrac{R_s}{L_s}i_q - \dfrac{1}{L_s}n_p\Omega_r\left(L_s i_d + \varphi_f\right) - \dfrac{1}{L_s}\left(V_{q,par} + V_{q,dead}\right) \end{cases}, \tag{1}$$

where i_d and i_q represent the *dq*-axes stator currents; u_d^* and u_q^* denote the *dq*-axes reference voltages; Ω_r is the mechanical rotational speed of the rotor; n_p is the number of pole pairs; $V_{d,par}$ and $V_{q,par}$ are the *dq*-axes disturbance induced by parametric uncertainties; $V_{d,dead}$ and $V_{q,dead}$ indicate *dq*-axes disturbances induced by inverter nonlinearity, and they are the sixth-order harmonic component in the synchronous rotating coordinate frame [34]; R_s, L_s, and φ_f denote the nominal values of stator resistance, stator inductance, and permanent magnet flux linkage, respectively; and R, L, and φ denote their actual values.

The electromagnetic torque of SMPMSM is expressed as

$$T_e = \frac{3}{2}n_p\varphi i_q . \tag{2}$$

The electromechanical equation is defined as

$$\frac{d\Omega_r}{dt} = \frac{T_e - T_L - B\omega_r}{J}, \tag{3}$$

where T_L, J, and B denote load torque, moment of inertia, and combined viscous friction, respectively.

B. Ultra-local Model of SMPMSM Drive System

The first-order ultra-local model [27] of a single-input single-output system is expressed as

$$\frac{dy}{dt} = F + \alpha u, \tag{4}$$

where u and y denote the control and output variables, respectively; α is a non-physical scaling factor selected by the designer; and F refers to the known and unknown parts of the system.

dq-Axes stator voltages u_d and u_q are replaced with u_d^* and u_q^*, and the disturbance voltages caused by inverter nonlinearity are considered as part of F. The output variables are i_d and i_q. The data-driven ultra-local model of SMPMSM drive system is designed as

$$\begin{cases} \dfrac{di_d}{dt} = F_d + \alpha_d u_d^* \\ \dfrac{di_q}{dt} = F_q + \alpha_q u_q^* \end{cases}, \tag{5}$$

and Eq. (5) can be represented by

$$\frac{d\boldsymbol{i}_{dq}}{dt} = \boldsymbol{F}_{dq} + \boldsymbol{\alpha}_{dq}\boldsymbol{u}_{dq}^*, \tag{6}$$

with $\boldsymbol{i}_{dq} = \begin{bmatrix} i_d \\ i_q \end{bmatrix}$, $\boldsymbol{F}_{dq} = \begin{bmatrix} F_d \\ F_q \end{bmatrix}$, $\boldsymbol{\alpha}_{dq} = \begin{bmatrix} \alpha_d & 0 \\ 0 & \alpha_q \end{bmatrix}$, and $\boldsymbol{u}_{dq}^* = \begin{bmatrix} u_d^* \\ u_q^* \end{bmatrix}$,

where α_d and α_q represent the scaling factors of dq-axes stator input voltages; and F_d and F_q denote the known and unknown parts, respectively.

C. Design of MFDPCC

The control timing of MFDPCC is described as follows. During the (k)th control period, the stator current $\boldsymbol{i}_{dq}[k]$ is sampled at the starting time. Then, the (k)th control period reference voltage $\boldsymbol{u}_{dq}^*[k]$ is calculated using the proposed MFDPCC and updated at the ending time of the (k)th control period. Reference voltage $\boldsymbol{u}_{dq}^*[k]$ is applied to control SMPMSM at the (k+1)th control period, and stator current $\boldsymbol{i}_{dq}[k+2]$ is generated. The delay of current sampling and reference voltage generation is one control period. Therefore, the total control delay is two control periods [35].

The changes in F_d and F_q within a short period are negligible when the control period is sufficiently small. Similar to [9], the reference voltage is assumed as a constant over two adjacent control periods, and the discretization of Eq. (6) is conducted from the starting time of the (k)th control period to the (k+2)th control period, which is given as

$$\boldsymbol{i}_{dq}[k+2] = \boldsymbol{i}_{dq}[k] + 2T\left(\boldsymbol{F}_{dq}[k] + \boldsymbol{\alpha}_{dq}\boldsymbol{u}_{dq}^*[k]\right), \tag{7}$$

where $\boldsymbol{i}_{dq}[k+2] = \begin{bmatrix} i_d[k+2] \\ i_q[k+2] \end{bmatrix}$, $\boldsymbol{i}_{dq}[k] = \begin{bmatrix} i_d[k] \\ i_q[k] \end{bmatrix}$, $\boldsymbol{F}_{dq}[k] = \begin{bmatrix} F_d[k] \\ F_q[k] \end{bmatrix}$, $\boldsymbol{u}_{dq}^*[k] = \begin{bmatrix} u_d^*[k] \\ u_q^*[k] \end{bmatrix}$, T is the control period, and the symbol "$[k]$" denotes the value at the (k)th control period.

To achieve current tracking at the starting time of the (k+2)th control period, current $\boldsymbol{i}_{dq}[k+2]$ is considered as the reference current. When Eq. (7) is used, the control voltage $\boldsymbol{u}_{dq}^{**}[k]$ of the dq-axes is predictably obtained as [3]

$$\boldsymbol{u}_{dq}^{**}[k] = \frac{1}{2T}\boldsymbol{\alpha}_{dq}^{-1}\left(\boldsymbol{i}_{dq}^*[k+2] - \boldsymbol{i}_{dq}[k]\right) - \boldsymbol{\alpha}_{dq}^{-1}\boldsymbol{F}_{dq}[k], \tag{8}$$

where $\boldsymbol{u}_{dq}^{**}[k] = \begin{bmatrix} u_d^{**}[k] \\ u_q^{**}[k] \end{bmatrix}$ and $\boldsymbol{i}_{dq}^*[k+2] = \begin{bmatrix} i_d^*[k+2] \\ i_q^*[k+2] \end{bmatrix}$.

Under the assumption that the estimation of $\boldsymbol{F}_{dq}[k]$ is accurate, the control voltage $\boldsymbol{u}_{dq}^{**}[k]$ of the dq-axes is written as

$$\boldsymbol{u}_{dq}^{**}[k] = \frac{1}{2T}\boldsymbol{\alpha}_{dq}^{-1}\left(\boldsymbol{i}_{dq}^*[k+2] - \boldsymbol{i}_{dq}[k]\right) - \boldsymbol{\alpha}_{dq}^{-1}\hat{\boldsymbol{F}}_{dq}[k], \tag{9}$$

where $\hat{\boldsymbol{F}}_{dq}[k] = \begin{bmatrix} \hat{F}_d[k] \\ \hat{F}_q[k] \end{bmatrix}$, and the symbol "$\hat{}$" denotes the estimation value.

The maximum magnitude of the output voltage of the space vector PWM inverter limited by the DC-link voltage is $U_{dc}/\sqrt{3}$ within the linear modulation range. However, the magnitude of the reference voltage may exceed the maximum value during the transient process. Once this condition occurs, the phase angle of the reference voltage is kept constant based on the minimum phase error method [36], and the reference voltage is modified as

$$\boldsymbol{u}_{dq}^*[k] = \begin{cases} \dfrac{U_{dc}/\sqrt{3}}{u_s[k]}\boldsymbol{u}_{dq}^{**}[k] & u_s[k] > \dfrac{U_{dc}}{\sqrt{3}} \\ \boldsymbol{u}_{dq}^{**}[k] & u_s[k] \le \dfrac{U_{dc}}{\sqrt{3}} \end{cases}, \tag{10}$$

where U_{dc} denotes the DC-link voltage,

$u_s[k] = \sqrt{\left(u_d^{**}[k]\right)^2 + \left(u_q^{**}[k]\right)^2}$, and $\boldsymbol{u}_{dq}^*[k] = \begin{bmatrix} u_d^*[k] \\ u_q^*[k] \end{bmatrix}$.

A model of the system is required to analyze the stability of the proposed method. However, the ultra-local model is used because the proposed method is not designed based on

the mathematical model of SMPMSM drive system. The discretization of the ultra-local model is conducted from the (k+1)th to the (k+2)th control periods and given as

$$\boldsymbol{i}_{dq}[k+2]=\boldsymbol{i}_{dq}[k+1]+T\left(\boldsymbol{F}_{dq}[k+1]+\boldsymbol{\alpha}_{dq}\boldsymbol{u}_{dq}^{*}[k]\right). \quad (11)$$

The control voltage in Eq. (9) is substituted as the reference voltage into Eq. (11) by disregarding reference voltage modification during the transient process. Then, the following is obtained:

$$\boldsymbol{i}_{dq}[k+2]=\boldsymbol{i}_{dq}[k+1]+T\left(\boldsymbol{F}_{dq}[k+1]+\left(\frac{1}{2T}\left(\boldsymbol{i}_{dq}^{*}[k+2]-\boldsymbol{i}_{dq}[k]\right)-\hat{\boldsymbol{F}}_{dq}[k]\right)\right). \quad (12)$$

The algebraic parameter identification techniques used to estimate F_{dq}[k] are non-asymptotic, which eliminates the initial condition of the controlled system. Therefore, the estimated results immediately follow the accurate value [37]. With the assumption that the online estimation of F_{dq}[k] is accurate and F_{dq} can be considered the same between two consecutive control periods, then Eq. (12) is simplified into

$$\boldsymbol{i}_{dq}[k+2]=\boldsymbol{i}_{dq}[k+1]+\frac{1}{2}\left(\boldsymbol{i}_{dq}^{*}[k+2]-\boldsymbol{i}_{dq}[k]\right). \quad (13)$$

The closed-loop transfer function in discrete domain is obtained and given as

$$\frac{\boldsymbol{i}_d(z)}{\boldsymbol{i}_d^{*}(z)}=\frac{z^2}{2z^2-2z+1},\qquad \frac{\boldsymbol{i}_q(z)}{\boldsymbol{i}_q^{*}(z)}=\frac{z^2}{2z^2-2z+1}. \quad (14)$$

The poles of the transfer function is located in the stability boundary (the unit circle |z| = 1). Therefore, the closed-loop system is stable.

D. Online Estimation of F

On the basis of algebraic parameter identification techniques [38] and assuming that F is approximated by a constant function $\hat{F}$ with a short time interval, Eq. (4) can be rewritten in the operational domain, which may be regarded as Laplace transform and expressed as

$$sY=\frac{\hat{F}}{s}+\alpha U+y_0, \quad (15)$$

where $\hat{F}$ is a constant, and y_0 is the initial condition that can be eliminated by taking a derivative with respect to s.

$$Y+s\frac{dY}{ds}=-\frac{\hat{F}}{s^2}+\alpha\frac{dU}{ds} \quad (16)$$

To attenuate noise, both sides of Eq. (16) is multiplied by s^{-2} as follows:

$$s^{-4}\hat{F}=-s^{-2}Y-s^{-1}\frac{dY}{ds}+s^{-2}\alpha\frac{dU}{ds}. \quad (17)$$

The equivalence between d/ds and the multiplication by $-t$ in the time domain are considered. Hence, the inverse transform of Eq. (17) within a short time interval [0, T_F] is given as

$$\begin{aligned}\frac{T_F^3}{3!}\hat{F}&=-\int_0^{T_F}\int_0^{\delta}y(\tau)d\tau d\delta-\int_0^{T_F}(-\delta)y(\delta)d\delta\\&\quad+\int_0^{T_F}\int_0^{\delta}\alpha(-\tau)u(\tau)d\tau d\delta\\&=-\int_0^{T_F}d\tau\int_{\tau}^{T_F}y(\tau)d\delta-\int_0^{T_F}(-\delta)y(\delta)d\delta\\&\quad+\int_0^{T_F}d\tau\int_{\tau}^{T_F}\alpha(-\tau)u(\tau)d\delta\\&=-\int_0^{T_F}(T_F-\delta)y(\delta)d\delta-\int_0^{T_F}(-\delta)y(\delta)d\delta\\&\quad+\int_0^{T_F}\alpha(-\delta)(T_F-\delta)u(\delta)d\delta\\&=-\int_0^{T_F}\left((T_F-2\delta)y(\delta)+\alpha\tau(T_F-\delta)u(\delta)\right)d\delta\\\hat{F}&=-\frac{3!}{T_F^3}\int_0^{T_F}\left((T_F-2\delta)y(\delta)+\alpha\delta(T_F-\delta)u(\delta)\right)d\delta.\end{aligned} \quad (18)$$

$T_F = n_F T$ is defined, and n_F is the window sequence length. The input and output data are sampled in each control period and denoted by $u[0],\ldots,u[n_F]$ and $y[0],\ldots,y[n_F]$, respectively.

Let $f(\delta)=(T_F-2\delta)y(\delta)+\alpha\delta(T_F-\delta)u(\delta)$. Then, the numerical solution for the first-order integrator in Eq. (18) is achieved using the compound trapezoidal formula, and its digital implementation is given as

$$\begin{aligned}\hat{F}&=-\frac{3!}{(n_FT)^3}\int_0^{n_FT}f(\delta)d\delta\\&=-\frac{3!}{(n_FT)^3}\left(\int_0^{T}f(\delta)d\delta+\cdots+\int_{(n_F-1)T}^{n_FT}f(\delta)d\delta\right)\\&=-\frac{3!}{(n_FT)^3}\left(\frac{T}{2}\left(f(0)+f(T)\right)+\cdots+\frac{T}{2}\left(f\left((n_F-1)T\right)+f(n_FT)\right)\right)\\&=-\frac{3!}{(n_FT)^3}\left(\frac{T}{2}\left((n_FT-0)y[0]+\alpha\cdot0\cdot(n_FT-0)u[0]+(n_FT-2T)y[1]+\alpha T(n_FT-T)u[1]\right)+\cdots\right.\\&\quad+\frac{T}{2}\left((n_FT-2(n_F-1)T)y[n_F-1]+\alpha(n_F-1)T(n_FT-(n_F-1)T)u[n_F-1]+(n_FT-2n_FT)y[n_F]+\alpha n_FT(n_FT-n_FT)u[n_F]\right)\\&=-\frac{3}{n_F^3T}\sum_{m=1}^{n_F}\left(\left((n_F-2(m-1))\times y[m-1]+\alpha(m-1)T(n_F-(m-1))\times u[m-1]+(n_F-2m)\times y[m]+\alpha mT(n_F-m)\times u[m]\right)\right),\end{aligned} \quad (19)$$

where "m" represents the (m)th sampling point.

The (k-2)th control period reference voltages generate the (k)th control period stator currents based on the analysis of the control timing of MFDPCC. Hence, the estimation of $\hat{F}_d$ at the (k)th control period can be deduced from Eq. (19) by using the data from the predefined time window and represented as

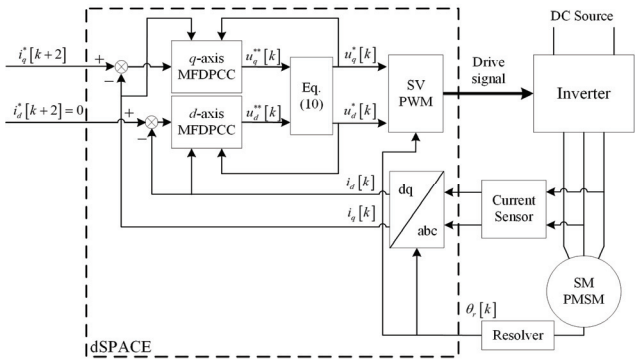

Fig. 1. Structure diagram of the SMPMSM drive system with MFDPCC.

$$\hat{F}_d[k] = -\frac{3}{n_F^3 T}\sum_{m=1}^{n_F}\Big(\big(\big(n_F - 2(m-1)\big)\times y[m-1] + \alpha_d (m-1)T\big(n_F-(m-1)\big)\times u[m-1] + \big(n_F - 2m\big)\times y[m] + \alpha_d mT\big(n_F - m\big)\times u[m]\Big), \tag{20}$$

with $\begin{cases} u[0] = u_d^*[k-n_F-2] \\ \vdots \\ u[n_F] = u_d^*[k-2] \end{cases}$, $\begin{cases} y[0] = i_d[k-n_F] \\ \vdots \\ y[n_F] = i_d[k] \end{cases}$.

$\hat{F}_q[k]$ is given as

$$\hat{F}_q[k] = -\frac{3}{n_F^3 T}\sum_{m=1}^{n_F}\Big(\big(\big(n_F - 2(m-1)\big)\times y[m-1] + \alpha_q (m-1)T\big(n_F-(m-1)\big)\times u[m-1] + \big(n_F - 2m\big)\times y[m] + \alpha_q mT\big(n_F - m\big)\times u[m]\Big), \tag{21}$$

with $\begin{cases} u[0] = u_q^*[k-n_F-2] \\ \vdots \\ u[n_F] = u_q^*[k-2] \end{cases}$, $\begin{cases} y[0] = i_q[k-n_F] \\ \vdots \\ y[n_F] = i_q[k] \end{cases}$.

When Eqs. (9), (10), (20), and (21) are combined, the *dq*-axes of MFDPCCs are designed, and the structure diagram of the SMPMSM drive system based on the proposed MFDPCC is shown in Fig. 1.

III. System Modeling and Simulation

Simulations were performed to demonstrate the effectiveness of the proposed MFDPCC and to compare it with the conventional decoupling PI current controller [39] and the model-based deadbeat predictive current controller (MBDPCC) [3]. The tested scheme is torque control; hence, no speed loop exists and the velocity of the SMPMSM drive system is controlled by a dynamometer. No additional inverter nonlinear compensation scheme is used for all the three methods. The nominal SMPMSM and the controller parameters are shown in Tables I and II.

The feedback current and the nominal SMPMSM parameters are used for feedforward decoupling and to design the gains of the PI current controller. Moreover, the PI-controlled SMPMSM system does not have any inverter nonlinearity compensation scheme. Then, the trade-off should be weighed between fast dynamic response and overshoot [35], and the desired bandwidth ω_{cc} of the PI current loop is set as 400 Hz (2512 rad/s). Finally, $K_p = \omega_{cc}L_s = 2.51$ and $K_i = \omega_{cc}R_s = 240.52$ are selected for the two *dq*-axes (the parallel type PI controller) [40].

TABLE I
Motor Specifications

Rated current	19 A_{rms}
Rated torque	13 N·m
Rated speed	500 rpm
Number of pole pairs	12
Magnetic flux	0.027 Wb
Moment of inertia	0.01015 kg.m^2
Stator resistance	0.0957 Ω
Stator inductance	1 mH

TABLE II
Control Parameters

Sampling time of PI controller	100 μs
Sampling time of MFDPCC	100 μs
Sampling time of MBDPCC	100 μs
Switching frequency of inverter	10 kHz
DC voltage	48 V

The guidelines for the selection of the control parameters of the proposed MFDPCC are described as follows.

1) α_d is selected, such that di_d/dt and $\alpha_d u_d^*$ are of the same order of magnitude, which is the same with α_q [27]. Moreover, α_d and α_q can be the same by comparing the mathematical model and the ultra-local model of the SMPMSM driving system, and the initial value can be set as $1/L_s$ due to the same scaling factor of the reference voltages of the *dq*-axes. Increasing α_d and α_q can improve the current dynamic response. However, large overshoots may occur. Therefore, $\alpha_d = \alpha_q = 750$ is finally selected to avoid overshoots and to consider the current dynamic response.

2) In [41], a short data window leads to good precision of the ultra-local model. However, this condition indicates that only a limited number of input and output is used, and the ultra-local model may not be accurately established. By contrast, data window length should be less than the electrical time constant. Therefore, window length can be normally selected as 5 to 20 times that of the control period of the current loop. When all these factors are considered, $n_F = 10$ is selected for the proposed SMPMSM drive system.

The first simulation is the comparison among the step current responses of the PI current controller, MBDPCC, and the proposed MFDPCC without parametric uncertainties and inverter nonlinearity. The rotating speed of SMPMSM is 100

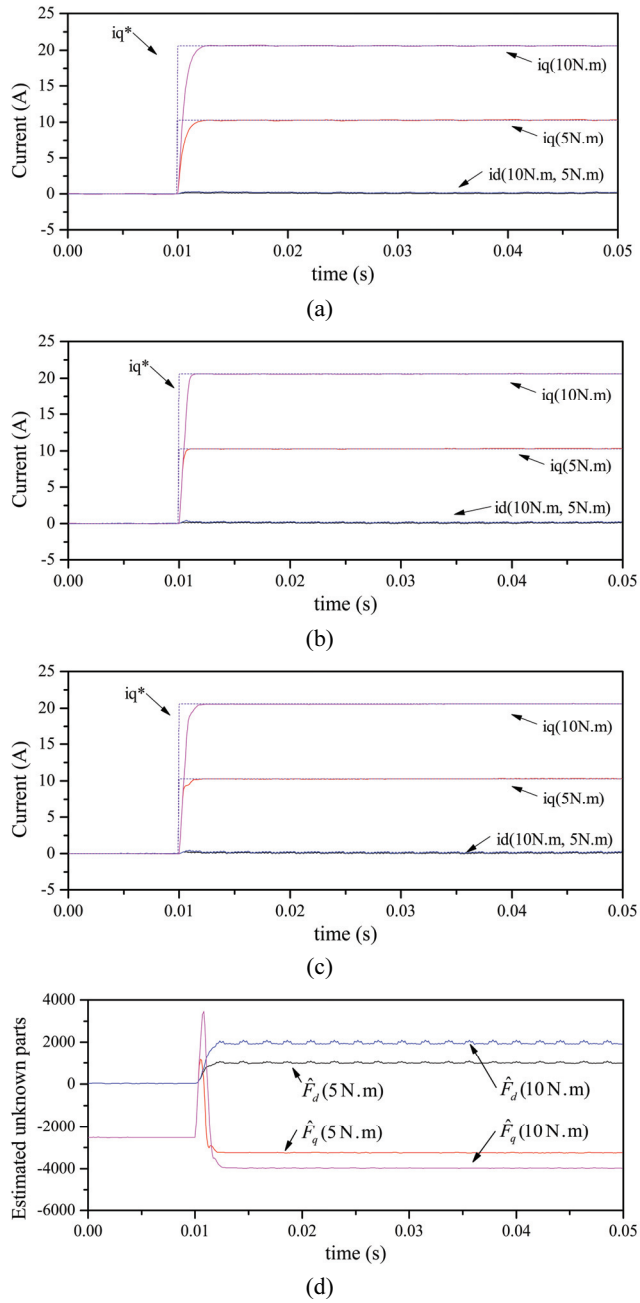

Fig. 2. Step current response at 100 r/min without parametric uncertainties and inverter nonlinearity (simulation): (a) PI controller with feedforward decoupling compensation. (b) MBDPCC. (c) Proposed MFDPCC. (d) Online estimation of F_d and F_q.

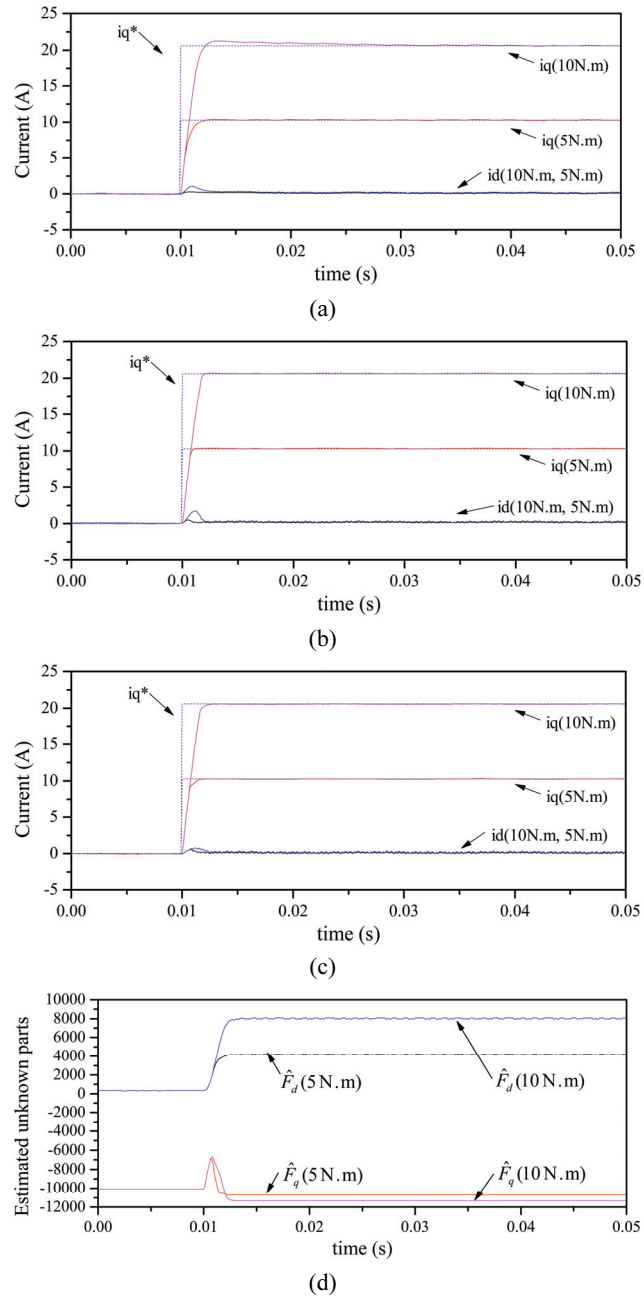

Fig. 3. Step current response at 400 r/min without parametric uncertainties and inverter nonlinearity (simulation): (a) PI controller with feedforward decoupling compensation. (b) MBDPCC (c) Proposed MFDPCC. (d) Online estimation of F_d and F_q.

r/min (20 Hz) and 400 r/min (80 Hz). Furthermore, the q-axis reference current, i.e., 10.2881 A (5 N.m) and 20.5761 A (10 N.m), is added at 0.01 s, and i_d^* is constantly maintained at zero. The current responses are shown in Figs. 2 and 3, and no significant difference is found between the proposed MFDPCC and the other two schemes.

The second simulation is the comparison among the step current responses of the three controllers with parametric uncertainties and inverter nonlinearity. The SMPMSM parameters are set as follows: R = 1.4 R_s, L = 0.8 L_s, and φ = 0.8 φ_f. Moreover, only dead time is included in the model and is set to 2 μs. Figs. 4 and 5 show the simulation results of the three schemes. The q-axis current rising time of the PI current controller is evidently increased. In Figs. 4b and 5b, MBDPCC exhibits rapid current response. However, a steady-state error occurs in the q-axis current under parametric uncertainties. As shown in Figs. 4c and 5c, MFDPCC has no overshoot, exhibits faster transient response, and has a lower steady-state current

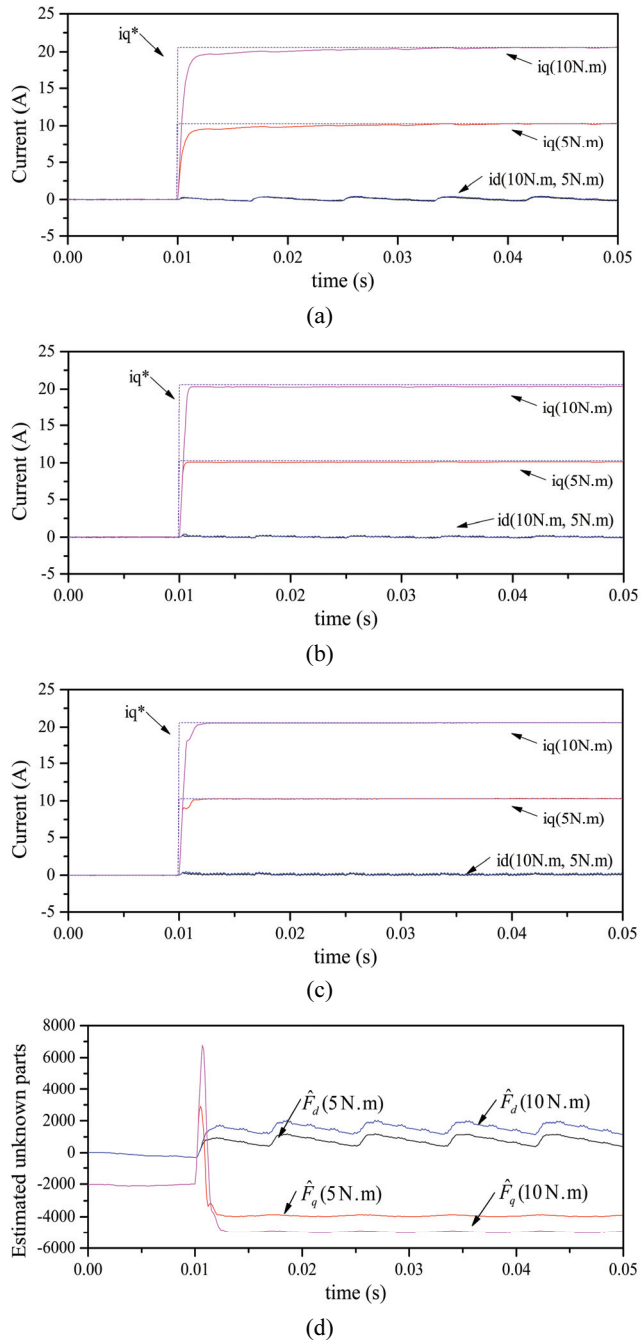

Fig. 4. Step current response at 100 r/min with parametric uncertainties and inverter nonlinearity (simulation): (a) PI controller with feedforward decoupling compensation. (b) MBDPCC. (c) Proposed MFDPCC. (d) Online estimation of F_d and F_q.

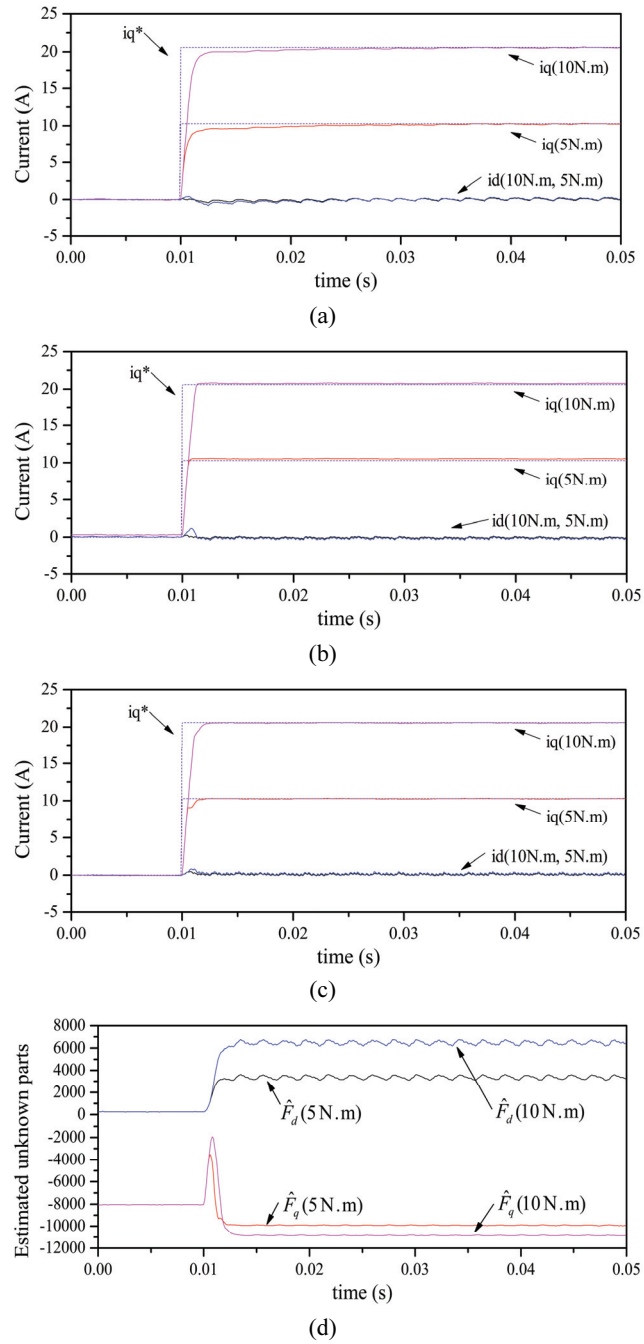

Fig. 5. Step current response at 400 r/min with parametric uncertainties and inverter nonlinearity (simulation): (a) PI controller with feedforward decoupling compensation. (b) MBDPCC. (c) Proposed MFDPCC. (d) Online estimation of F_d and F_q.

ripple. On the basis of the analysis, $\hat{F}_d$ and $\hat{F}_q$ contain the disturbance caused by parametric uncertainties and inverter nonlinearity. From Figs. 4d and 5d, the pulsation components appear in $\hat{F}_d$ and $\hat{F}_q$, and the frequencies of the pulsation components are 120 Hz and 480 Hz, which is six times the driving frequency induced by inverter nonlinearity. Moreover, the static values of $\hat{F}_d$ and $\hat{F}_q$ differ from those in the first simulation because of parametric uncertainties. Therefore, the disturbances caused by parametric uncertainties and inverter nonlinearity can be effectively eliminated by using the proposed MFDPCC.

The magnitude of the disturbance caused by inverter nonlinearity is dependent on the dead time, nonlinear characteristics, and parasitic capacity of the semiconductor

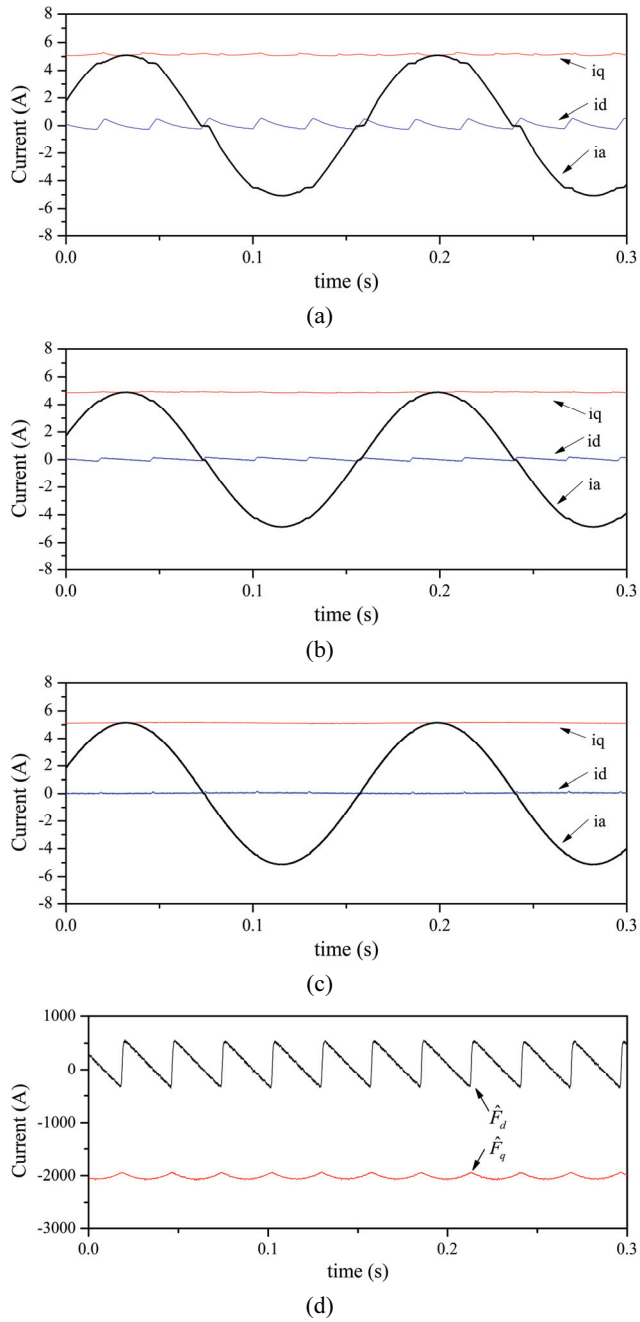

Fig. 6. Steady-state current response at 30 r/min with parametric uncertainties and inverter nonlinearity (simulation): (a) PI controller with feedforward decoupling compensation. (b) MBDPCC. (c) Proposed MFDPCC. (d) Online estimation of F_d and F_q.

device. Therefore, the distortion is severe at low-speed and light-load conditions.

The third simulation is the steady-state current response under inverter nonlinearity with the same parameter variations at 30 r/min and the reference currents are $i_d^* = 0$ A and $i_q^* = 5.15$ A (2.5 N.m). The simulation result is shown in Fig. 6, and the total harmonic distortion (THD) of the a-phase stator current is summarized in Table III. Evidently, the a-phase

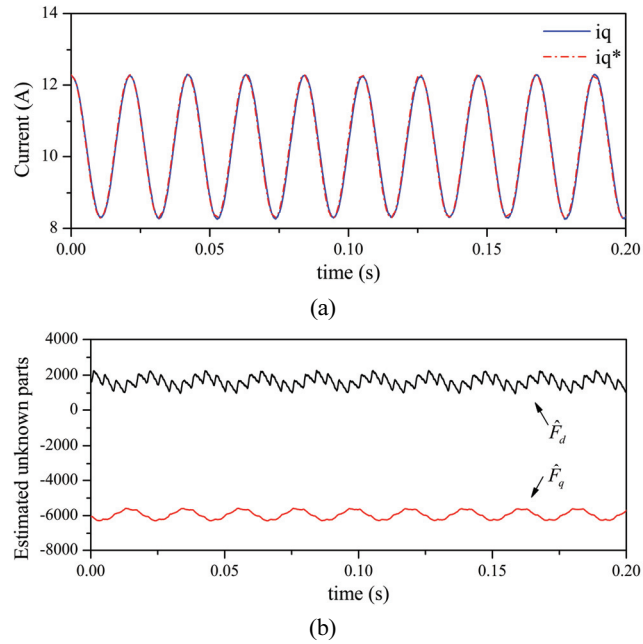

Fig. 7. Current response under the sinusoidal q-axis reference current at 200 r/min (simulation): (a) q-Axis reference and measured currents. (b) Online estimation of F_d and F_q.

TABLE III
THD OF a-PHASE STATOR CURRENT (SIMULATION)

PI	4.48%
MBDPCC	1.47%
MFDPCC	0.62%

current is distorted and the d-axis current contains the sixth-order harmonic component caused by inverter nonlinearity when the PI current controller and MBDPCC are used. Compared with the proposed MFDPCC, the harmonics of the dq-axes and a-phase stator currents are effectively reduced because $\hat{F}_d$ and $\hat{F}_q$ include the sixth-order harmonic component due to inverter nonlinearity shown in Fig. 6d.

The fourth simulation is the current response of the proposed method under the sinusoidal q-axis reference current at 200 r/min and the disturbance is the same as that in the third simulation. The q-axis reference current is set as the DC component, which superimposes a sinusoidal component. The DC q-axis reference current is 10.2881 A. Moreover, the angular frequency of the sinusoidal component is 300 rad/s and the amplitude is 2 A. Fig. 7 shows the simulation results of the proposed MFDPCC. Evidently, the actual q-axis currents can follow the reference well.

IV. EXPERIMENTAL RESULTS

Fig. 8 shows the experimental setup to verify the effectiveness of the proposed method. SMPMSM is coupled with a 2.2 kW AC induction motor dynamometer, and is

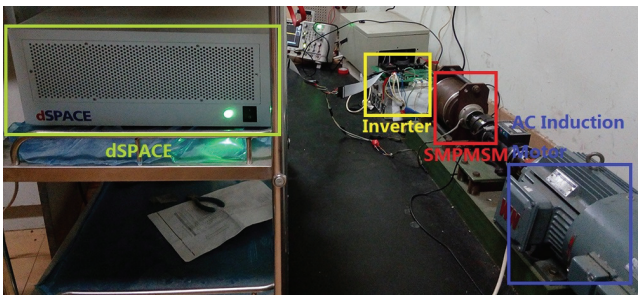

Fig. 8. Experimental bench of the SMPMSM drive system.

connected to a metal–oxide–semiconductor field-effect transistor (MOSFET) module inverter. The dead time of the inverter is set as 2 μs, and dSPACE/DS1007 with DS5202 is used as the inverter controller. The rotor position is measured using one pair of pole resolvers, and the Hall effect current sensor is LEM LA25-P. The currents $\hat{F}_d$ and $\hat{F}_q$ of the *dq*-axes are transmitted by dSPACE/ControlDesk, and phase current is measured with the current probe of an oscilloscope. As suggested previously, the induction motor drive system is working under the speed control mode, and the tested SMPMSM drive system is working under the torque control mode. The nominal machine and controller parameters are the same as those used in the simulation and listed in Tables I and II. Moreover, compared with the two other schemes, the calculation time of the proposed MFDPCC has increased by approximately 5 μs in dSPACE by using the double-precision floating point data type. To evaluate the current control performance of the proposed MFDPCC, step and steady-state current response tests are conducted.

The test condition of the experiment is the same as that in the second simulation. However, the actual motor parameters and the nonlinearity of the inverter are unavailable. The step current responses of the three methods are shown in Figs. 9 and 10. The settling time of the PI current controller is longer compared with those of the other two methods, and the *dq*-axes currents are distorted severely due to inverter nonlinearity. The steady-state current response of MBDPCC is worse than that in the simulation due to parametric uncertainties and inverter nonlinearity. However, the proposed MFDPCC exhibits its superior transient and steady-state current responses. This finding illustrates that parametric uncertainties and inverter nonlinearity have minimal effects on the performance of the proposed controller. $\hat{F}_d$ and $\hat{F}_q$ are shown in Figs. 9d and 10d, respectively. Apparently, the steady-state values of $\hat{F}_d$ and $\hat{F}_q$ differ from those in the simulation because the uncertainties in a real system are distinct from those in the simulation. Moreover, $\hat{F}_d$ and $\hat{F}_q$ contain the sixth-order harmonic component caused by inverter nonlinearity.

A long time axis is used to fully present the transient responses of $\hat{F}_d$ and $\hat{F}_q$, and the convergence time is 90 ms in the experiment compared with 3 ms in the simulation. The

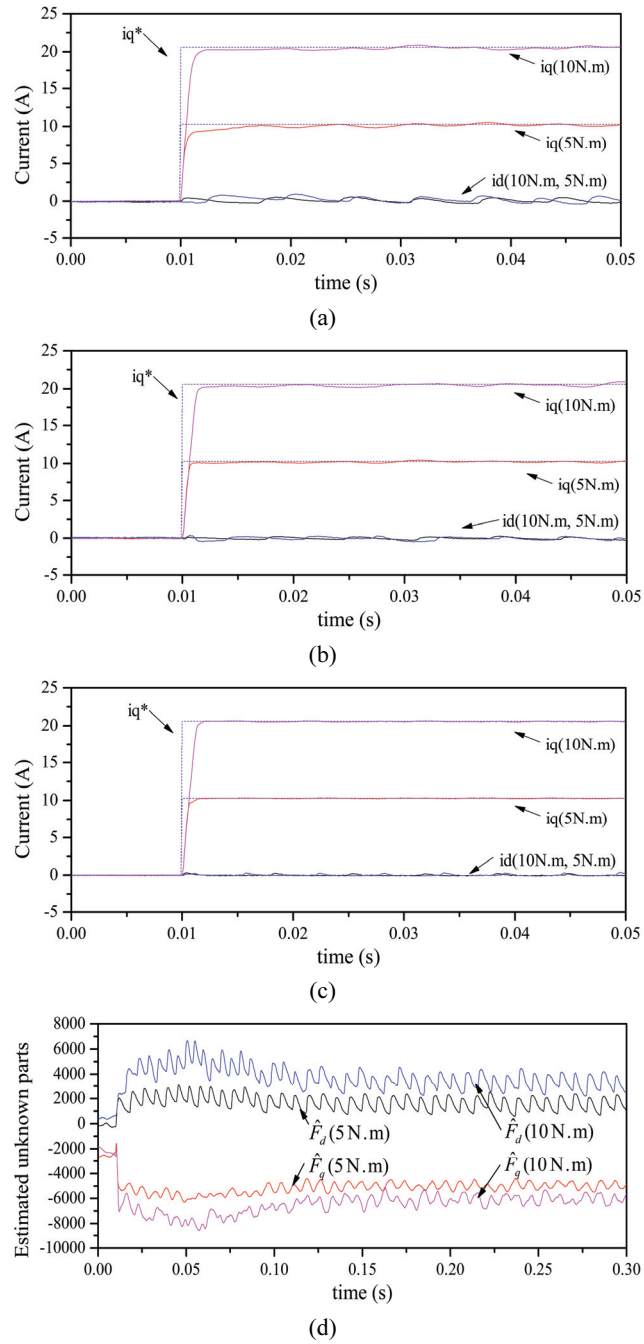

Fig. 9. Step current response at 100 r/min (experiment): (a) PI controller with feedforward decoupling compensation. (b) MBDPCC. (c) Proposed MFDPCC. (d) Online estimation of F_d and F_q.

speed of SMPMSM in the simulation is controlled by an ideal dynamometer and is kept constant under the condition of abrupt load change (i.e., the *q*-axis step current of SMPMSM). However, the speed of the SMPMSM system in the experiment is controlled by an AC induction motor fed by an inverter (ABB ACS600). Therefore, the speed dynamic response is limited by the induction motor drive system. The speed disturbance of the induction motor will certainly occur under a

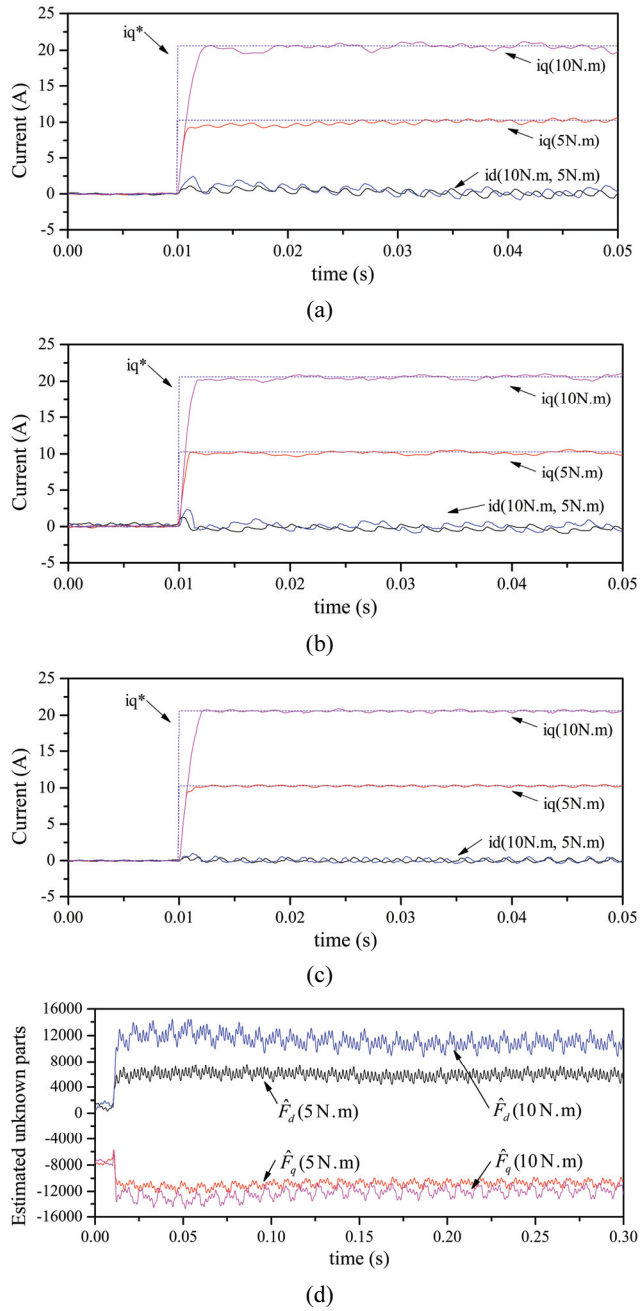

Fig. 10. Step current response at 400 r/min (experiment): (a) PI controller with feedforward decoupling compensation. (b) MBDPCC. (c) Proposed MFDPCC. (d) Online estimation of F_d and F_q.

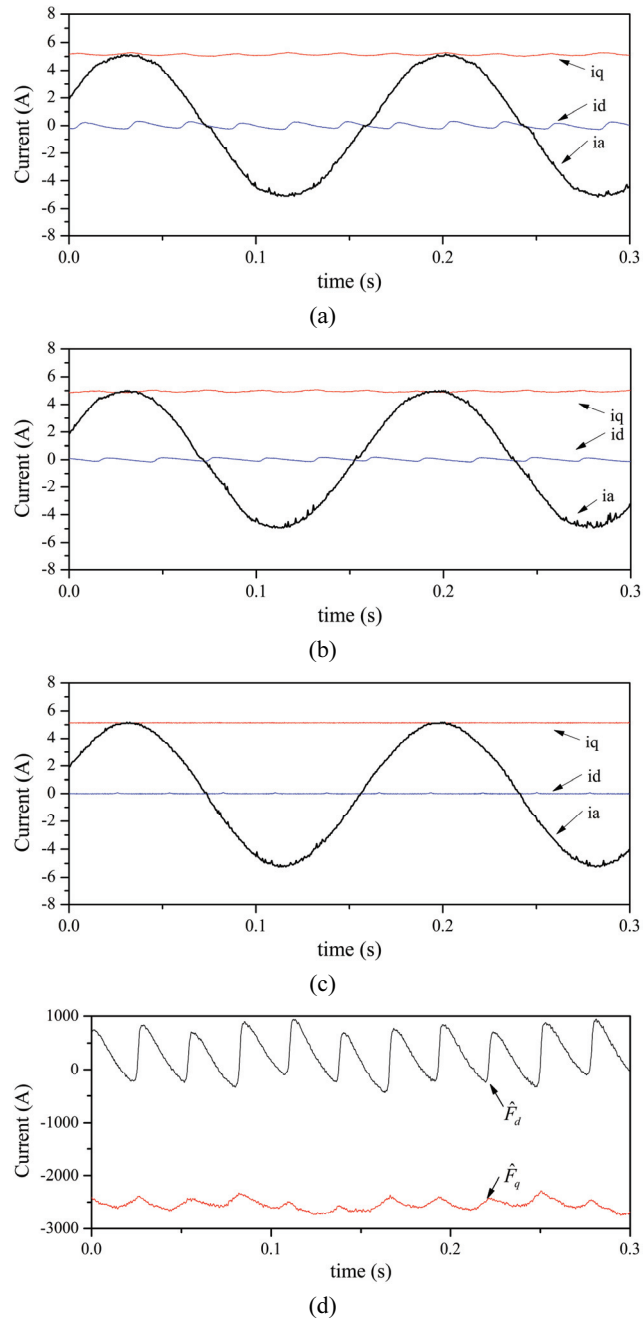

Fig. 11. Steady-state current response at 30 r/min (experiment): (a) PI controller with feedforward decoupling compensation. (b) MBDPCC. (c) Proposed MFDPCC. (d) Online estimation of F_d and F_q.

sudden external load torque application and results in a dynamic process of rotor speed. Eventually, $\hat{F}_d$ and $\hat{F}_q$, which include back-electromotive force related to rotor speed, will require more time to converge to their steady-state values.

The test condition is the same as that in the third simulation. Fig. 11 shows the experimental results of the steady-state current response at 30 r/min, which are consistent with the simulation results presented in Fig. 6. The THD of the *a*-phase stator current is presented in Table IV. The current harmonic caused by inverter nonlinearity with parametric uncertainties is effectively eliminated by the proposed MFDPCC even if the system operates under low-speed and light-load conditions. $\hat{F}_d$ and $\hat{F}_q$ reflect the disturbances caused by inverter

TABLE IV
THD OF *a*-PHASE STATOR CURRENT (EXPERIMENT)

PI	6.31%
MBDPCC	4.22%
MFDPCC	2.52%

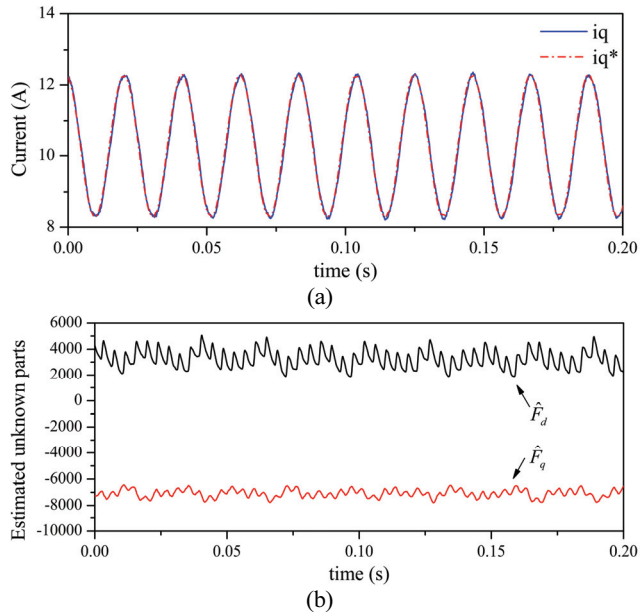

Fig. 12. Current response under the sinusoidal q-axis reference current at 200 r/min (experiment): (a) q-Axis reference and measured current. (b) Online estimation of F_d and F_q.

nonlinearity and parametric uncertainties.

Finally, the experiment for the proposed method is designed based on the fourth simulation. Fig. 12 shows the experimental results of the sinusoidal current response at 200 r/min. The results are clearly similar to those of the fourth simulation, and the current response of the proposed method is verified when tracking the sinusoidal reference current.

V. Conclusion

The ultra-local model of SMPMSM drive system that incorporates parametric uncertainties and inverter nonlinearity is first established by using input and output data. Subsequently, MFDPCC is proposed and designed based on deadbeat predictive current control. This method is a new means to control SMPMSM drive systems with parametric uncertainties and inverter nonlinearity and does not require any knowledge of SMPMSM drive system. Moreover, the controller parameters are simple to adjust. MFDPCC is evaluated on a simulation platform and an experimental test bench. Compared with the feedforward decoupling PI current controller and MBDPCC, MFDPCC exhibits faster transient performance and lower current pulsation in the steady state, and thus, it has effectively improved the dynamic and steady-state current performance of SMPMSM drive system. The proposed MFDPCC adopts an integrated solution by using the ultra-local model and deadbeat predictive current control to achieve high-performance current control and reliable operation of SMPMSM drive systems. In addition, the proposed MFDPCC exhibits the potential for interior PMSM application and as a replacement for the conventional PI current controller.

Acknowledgment

This research was supported by the National Natural Science Foundation of China (Grant No. 51377041).

References

[1] B. Stumberger, G. Stumberger, D. Dolinar, A. Hamler, and M. Trlep, "Evaluation of saturation and cross-magnetization effects in interior permanent-magnet synchronous motor," *IEEE Trans. Ind. Appl.,* Vol. 39, No. 5, pp. 1264-1271, Sep./Oct 2003.

[2] R. Ramakrishnan, R. Islam, M. Islam, and T. Sebastian, "Real time estimation of parameters for controlling and monitoring permanent magnet synchronous motors," in *IEEE International Electric Machines & Drives Conference*, pp. 1188-1193, 2009.

[3] P. Cortes, M. P. Kazmierkowski, R. M. Kennel, D. E. Quevedo, and J. Rodriguez, "Predictive control in power electronics and drives," *IEEE Trans. Ind. Electron.,* Vol. 55, No. 12, pp. 4312-4324, Dec. 2008.

[4] F. X. Wang, S. H. Li, X. Z. Mei, W. Xie, J. Rodriguez, and R. M. Kennel, "Model-based predictive direct control strategies for electrical drives: an experimental evaluation of PTC and PCC methods," *IEEE Trans. Ind. Informat.,* Vol. 11, No. 3, pp. 671-681, Jun 2015.

[5] F. Morel, X. Lin-Shi, J. M. Retif, B. Allard, and C. Buttay, "A comparative study of predictive current control schemes for a permanent-magnet synchronous machine drive," *IEEE Trans. Ind. Electron.,* Vol. 56, No. 7, pp. 2715-2728, Jul 2009.

[6] P. Wipasuramonton, Z. Q. Zhu, and D. Howe, "Predictive current control with current-error correction for PM brushless AC drives," *IEEE Trans. Ind. Appl.,* Vol. 42, No. 4, pp. 1071-1079, Jul./Aug. 2006.

[7] J. Castello Moreno, J. M. Espi Huerta, R. Garcia Gil, and S. A. Gonzalez, "A robust predictive current control for three-phase grid-connected inverters," *IEEE Trans. Ind. Electron.,* Vol. 56, No. 6, pp. 1993-2004, Jun. 2009.

[8] L.-H. Hoang, K. Slimani, and P. Viarouge, "Analysis and implementation of a real-time predictive current controller for permanent-magnet synchronous servo drives," *IEEE Trans. Ind. Electron.,* Vol. 41, No. 1, pp. 110-117, Feb. 1994.

[9] G. H. Bode, P. C. Loh, M. J. Newman, and D. G. Holmes, "An improved robust predictive current regulation algorithm," *IEEE Trans. Ind. Appl.,* Vol. 41, No. 6, pp. 1720-1733, Nov./Dec. 2005.

[10] W. Hongjia, X. Dianguo, and Y. Ming, "Improved deadbeat predictive current control strategy of permanent magnet motor drives," *Transactions of China Electrotechnical Societ,* Vol. 6, pp. 39-45, 2011.

[11] N. Li, Y. Ming, L. Keshu, and X. Dianguo, "A predictive current control scheme for permanent magnet synchronous motors," *Proceedings of the CSEE,* Vol. 6, pp. 131-137, 2012.

[12] S. J. Jeong and S. H. Song, "Improvement of predictive current control performance using online parameter estimation in phase controlled rectifier," *IEEE Trans. Power Electron.,* Vol. 22, No. 5, pp. 1820-1825, Sep. 2007.

[13] Y. A. R. I. Mohamed and E. F. El-Saadany, "An improved deadbeat current control scheme with a novel adaptive self-tuning load model for a three-phase PWM voltage-source inverter," *IEEE Trans. Ind. Electron.,* Vol. 54, No. 2, pp. 747-759, Apr 2007.

[14] G. Gatto, I. Marongiu, and A. Serpi, "Discrete-time parameter identification of a surface-mounted permanent magnet synchronous machine," *IEEE Trans. Ind. Electron.,* Vol. 60, No. 11, pp. 4869-4880, Nov. 2013.

[15] Y. A. R. I. Mohamed and F. El-Saadany, "Robust high bandwidth discrete-time predictive current control with predictive internal model – A unified approach for voltage-source PWM converters," *IEEE Trans. Power Electron.,* Vol. 23, No. 1, pp. 126-136, Jan. 2008.

[16] K. H. Kim, "Model reference adaptive control-based adaptive current control scheme of a PM synchronous motor with an improved servo performance," *IET Electric Power Appl.,* Vol. 3, No. 1, pp. 8-18, Jan. 2009.

[17] S. H. Chang, P. Y. Chen, Y. H. Ting, and S. W. Hung, "Robust current control-based sliding mode control with simple uncertainties estimation in permanent magnet synchronous motor drive systems," *IET Electric Power Appl.,* Vol. 4, No. 6, pp. 441-450, Jul 2010.

[18] J. Weigold and M. Braun, "Predictive current control using identification of current ripple," *IEEE Trans. Ind. Electron.,* Vol. 55, No. 12, pp. 4346-4353, Dec. 2008.

[19] C. K. Lin, T. H. Liu, J. T. Yu, L. C. Fu, and C. F. Hsiao, "Model-free predictive current control for interior permanent-magnet synchronous motor drives based on current difference detection technique," *IEEE Trans. Ind. Electron.,* Vol. 61, No. 2, pp. 667-681, Feb. 2014.

[20] Y. Chen, T. H. Liu, C. F. Hsiao, and C. K. Lin, "Implementation of adaptive inverse controller for an interior permanent magnet synchronous motor adjustable speed drive system based on predictive current control," *IET Electric Power Appl.,* Vol. 9, No. 1, pp. 60-70, Jan. 2015.

[21] C. K. Lin, J. T. Yu, Y. S. Lai, H. C. Yu, Y. H. Lin, and F. M. Chen, "Simplified model-free predictive current control for interior permanent magnet synchronous motors," *Electronics Lett.,* Vol. 52, No. 1, pp. 49-50, Jan. 2016.

[22] C. K. Lin, J. T. Yu, Y. S. Lai, and H. C. Yu, "Improved model-free predictive current control for synchronous reluctance motor drives," *IEEE Trans. Ind. Electron.,* Vol. 63, No. 6, pp. 3942-3953, Jun. 2016.

[23] A. Imura, T. Takahashi, M. Fujitsuna, T. Zanma, and S. Doki, "Refinement of inverter model considering dead-time for performance improvement in predictive instantaneous current control," *IEEJ Trans. Electr. Electron. Eng.,* Vol. 9, No. 1, pp. 83-89, Jan. 2014.

[24] A. Imura, T. Takahashi, M. Fujitsuna, T. Zanma, and S. Doki, "Improved PMSM model considering flux characteristics for model predictive-based current control," *IEEJ Trans. Electr. Electron. Eng.,* Vol. 10, No. 1, pp. 92-100, Jan. 2015.

[25] J. Q. Han, "From PID to active disturbance rejection control," *IEEE Trans. Ind. Electron.,* Vol. 56, No. 3, pp. 900-906, Mar. 2009.

[26] Z. S. Hou and S. T. Jin, "Data-driven model-free adaptive control for a class of MIMO nonlinear discrete-time systems," *IEEE Trans. Neural Netw.,* Vol. 22, No. 12, pp. 2173-2188, Dec. 2011.

[27] M. Fliess and C. Join, "Model-free control," *Int. J. Contr.,* Vol. 86, No. 12, pp. 2228-2252, Dec. 2013.

[28] R. E. Precup, M. B. Radac, C. A. Dragos, S. Preitl, and E. M. Petriu, "Model-free tuning solution for sliding mode control of servo systems," in *Annual IEEE Systems Conference*, pp. 30-35, 2014.

[29] R. Madonski and P. Herman, "Model-free control of a two-dimensional system based on uncertainty reconstruction and attenuation," in *International Conference on Control and Fault-Tolerant Systems*, pp. 542-547, 2013.

[30] J. De Miras, C. Join, M. Fliess, S. Riachy, and S. Bonnet, "Active magnetic bearing: A new step for model-free control," in *IEEE 52nd Annual Conference on Decision and Control*, pp. 7449-7454, 2013.

[31] M. B. Radac, R. C. Roman, R. E. Precup, and E. M. Petriu, "Data-driven model-free control of twin rotor aerodynamic systems: Algorithms and experiments," in *IEEE International Symposium on Intelligent Control*, pp. 1889-1894, 2014.

[32] F. Lafont, J.-F. Balmat, N. Pessel, and M. Fliess, "A model-free control strategy for an experimental greenhouse with an application to fault accommodation," *Computers and Electronics in Agriculture,* Vol. 110, pp. 139-149, Jan 2015.

[33] Y. Xu, E. Bideaux, and D. Thomasset, "Robustness study on the modelfree control and the control with restricted model of a high performance electro-hydraulic system," in *Scandinavian International Conference on Fluid Power*, 2013.

[34] D. M. Park and K. H. Kim, "Parameter-independent online compensation scheme for dead time and inverter nonlinearity in IPMSM drive through waveform analysis," *IEEE Trans.Ind. Electron.,* Vol. 61, No. 2, pp. 701-707, Feb 2014.

[35] H. J. Wang, M. Yang, L. Niu, and D. G. Xu, "Current-loop bandwidth expansion strategy for permanent magnet synchronous motor drives," *Proceedings of the 5th IEEE Conference on Industrial Electronics and Applications,* pp. 1340-1345, 2010.

[36] S. Lerdudomsak, S. Doki, and S. Okuma, "Voltage limiter calculation method for fast torque response of IPMSM in overmodulation range," *IEEJ Trans. Electr. Electron. Eng.,* Vol. 5, No. 5, pp. 586-595, Sep. 2010.

[37] J. R. Trapero, H. Sira-Ramirez, and V. F. Batlle, "An algebraic frequency estimator for a biased and noisy sinusoidal signal," *Signal Processing,* Vol. 87, No. 6, pp. 1188-1201, Jun 2007.

[38] M. Fliess and H. Sira-Ramírez, "Closed-loop parametric identification for continuous-time linear systems via new algebraic techniques," *Advances in Industrial Control,* pp. 363-391, 2008.

[39] S. Morimoto, M. Sanada, and Y. Takeda, "Wide-speed operation of interior permanent magnet synchronous motors with high-performance current regulator," *IEEE Trans. Ind. Appl.,* Vol. 30, No. 4, pp. 920-926, Jul./Aug. 1994.

[40] Y. C. Kwon, S. Kim, and S. K. Sul, "Voltage feedback current control scheme for improved transient performance

of permanent magnet synchronous machine drives," *IEEE Trans. Ind. Electron.,* Vol. 59, No. 9, pp. 3373-3382, Sep 2012.

[41] M. Fliess and C. Join, "Stability margins and model-free control: A first look," in *European Control Conference*, pp. 454-459, 2014.

Yanan Zhou was born in Anhui, China. He obtained his B.S. in Automation from Anhui University of Technology, Maanshan, China and his M.S. in Electrical Engineering from Hefei University of Technology, Hefei, China in 2005 and 2012, respectively. He is currently working on a Ph.D. degree in the Department of Electrical Engineering and Automation, Hefei University of Technology. He is an assistant research fellow in the Automotive Research Institute, Hefei University of Technology. His research interests include the predictive control and robust control of electrical motor drives.

Hongmei Li was born in Anhui, China in 1969. She obtained her B.S. and M.S. in Electrical Engineering from Hefei University of Technology in 1991 and 1996, respectively, and her Ph.D. in Electrical Engineering from Shenyang University of Technology in 2003. She has been a professor in the Department of Electrical Engineering, Hefei University of Technology since 2006. Her research interests include power electronics and motor control, fault diagnosis, and fault-tolerant control of electrical machine systems.

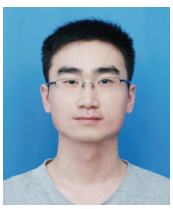

Hengguo Zhang was born in Hefei, China. He obtained his B.S. in Electrical Engineering from Hefei University of Technology, Hefei, China, in 2013. He is currently working on a Ph.D. in Electrical Engineering. His research interests include high-frequency soft-switching techniques, design and control techniques for power converters, magnetic design, and the optimization of electric vehicle battery charger.